JOURNAL OF PETROLEUM GEOMECHANICS
(JPG)

Original article

2D Simulation of Shale Gas Reservoir through Z-Axis Tipper Electromagnetic Data

Maysam Abedi[1*]

1- School of Mining Engineering, College of Engineering, University of Tehran, Tehran, Iran.

Received: 26 February 2024; Accepted: 28 September 2024

DOI: 10.22107/jpg.2025.445823.1229

Keywords

Shale gas, Unconventional reservoir, Resistivity, ZTEM, Inversion, Simulation

Abstract

Shale gas, an unconventional natural gas resource abundant in organic matter, has gained significant attention in global natural gas exploration as a crucial supplement and alternative to conventional natural gas sources. Due to higher electrical resistivity of oil traps in conductive sedimentary backgrounds, shale gas reservoirs are ideal targets for geophysical studies to be explored, whereby the Z-axis tipper electromagnetic method (ZTEM) can be employed to simulate and model their geoelectrical responses. The study conducted involved the utilization of an airborne method, a tool that relies on natural source transmitter, to simulate shale gas reservoirs. Initially, geoelectrical models of shallow shale gas reservoirs were constructed for three different simple geological scenarios, followed by the generation of responses through an airborne geophysical survey. The assumed electrical resistivity models were effectively reconstructed by applying an inversion algorithm to the data. This process proved to be successful in accurately representing the physical characteristics of shale gas reservoirs. As a result, this innovative tool offers the capability to rapidly explore vast areas with high potential for shale gas reserves, enabling the identification of valuable targets efficiently. The combination of advanced technology, numerical modeling and geological expertise allows for the expedited discovery of significant resources in the field of shale gas exploration.

1. Introduction

Petroleum hydrocarbons play a crucial role as a primary energy source on a global scale [1]. These hydrocarbons can be broadly categorized into conventional and unconventional types, based on their characteristics, geological formations, and extraction techniques. As conventional hydrocarbons are gradually depleting, the focus has shifted towards the exploitation of unconventional hydrocarbons for present and future energy production [2]. The abundance of unconventional hydrocarbon reserves has led to a significant shift in the exploration and utilization of these resources to meet the growing energy demands [3]. Additionally, conventional resources are being depleted at an alarming rate, and a significant amount of oil and gas has already been extracted through conventional means. However, advancements in technology have made the production of unconventional petroleum resources more feasible, contrary to their previous perception as unviable assets [4]. In recent years, there has been a notable increase in the significance of exploring and extracting unconventional hydrocarbon resources.

The geologic nature of the hydrocarbon reservoir plays a crucial role. As mentioned by Song et al. (2015) [3], unconventional resources are characterized by reservoirs with distinct geological properties. The complex petrophysical system associated with unconventional hydrocarbons, as highlighted by Hamada (2016) [4], further sets them apart. This complexity requires advanced technology and expertise for successful extraction. The extraction methods used for hydrocarbons vary between conventional

* **Corresponding Author:** MaysamAbedi@ut.ac.ir

and unconventional resources, as explained by Heikal (2008) [5]. Unconventional hydrocarbons require extra technology, energy, and capital investment for extraction since they lack the natural geological processes found in conventional reservoirs. These resources have lower porosity and permeability, necessitating stimulation and other techniques such as enhanced oil recovery (EOR) for effective production, as highlighted by Muther et al. (2022) [2]. Consequently, the economic cost of extracting unconventional hydrocarbons is significantly higher compared to conventional methods. However, due to their substantial global reserves, they remain promising prospects for future oil and gas production worldwide.

Unlike conventional gas reservoirs, which are relatively easy to extract, unconventional deposits present a more challenging environment for locating natural gas reserves. These unconventional deposits include coal beds, shales, low-quality reservoirs, and gas hydrates. However, extracting gas from these resources is not economically viable without certain techniques. For instance, hydraulic fractures or multilateral wellbores are used to stimulate the well and increase the flow rate. Generally, finding these resources is simpler because they are distributed horizontally, making them more accessible. Shale gas is a prime example of unconventional gas, where the natural gas remains trapped within the source rock instead of migrating to a porous reservoir. Shale, a sedimentary rock composed of fine-grained particles like clay, can be a valuable source of oil and natural gas. Unconventional gas, unlike traditional hydrocarbons, does not have its own natural pressure, therefore necessitating stimulation methods akin to those used in secondary recovery techniques in the conventional oil and gas sector.

Shale gas rocks possess a wide range of properties that can vary significantly, mainly due to the presence of clay minerals, high pressure from trapped fluids, and the inclusion of organic materials. These rocks have low porosity and extremely low permeability. However, it is important to note that the characteristics of shales, such as seismic anisotropy, mineral composition, total organic carbon (TOC) content, and porosity/permeability, can differ across different basins and even within the same basin, as highlighted by Sondergeld and Rai (2011) [6] and Roth (2010) [7]. The differentiation of shale lithology can be accomplished by analyzing the Vp/Vs ratio (compressive and shear seismic wave velocity) and P-Impedance. Reservoir shale can be distinguished from non-reservoir shale by considering both parameters together. Additionally, the estimation of gas saturation in shale reservoirs can be achieved by combining electrical resistivity with P-Impedance. Huang et al. highlighted in 2015 that the Vp/Vs ratio is the most effective parameter for identifying and evaluating shale gas reservoirs based on the results of logging [8]. Models for P-impedance and Vp/Vs ratio can be developed through amplitude versus angle (AVA) inversion of seismic data. Furthermore, electrical resistivity values can be obtained by inverting electromagnetic data, such as magnetotelluric (MT) and controlled-sourced electromagnetic (CSEM) data, as demonstrated by Kumar and Hoversten in 2012 [9]. In the context of shale gas, it is common for the resistivity to be higher than the background [10, 11], which provides valuable insights for reservoir characterization and evaluation. The seismic exploration methods for oil and gas in complex geologic environments have been complemented or provided with an alternative by the EM methods. Over the past two decades, the application of EM in hydrocarbon exploration has experienced significant growth. The journey began with the study of MT and has since transformed into the integration of CSEM as a significant asset in offshore exploration. Additionally, the onshore (land) EM technique known as the long offset transient electromagnetic (LOTEM) method has been developed, along with the multitransient electromagnetic (MTEM) method for both land and marine studies. These advancements have greatly expanded the capabilities and options available for exploring and discovering oil and gas resources [12-14].

Over the past decade, there have been significant advancements in electromagnetic exploration for unconventional oil and gas resources globally. These advancements include understanding the EM response mechanism of unconventional reservoir rocks, developing new methods for CSEM exploration on land and marine environments, and creating techniques for identifying and evaluating oil and gas using EM parameters. These cutting-edge technologies have been successfully utilized in the exploration and development of unconventional oil and gas

resources, gaining recognition from the petroleum geology and development communities. Notably, He and Wang (2007) have found that oil and gas reservoirs have high resistivity and polarization characteristics, while water-bearing reservoirs typically have low resistivity and high polarization [15]. By leveraging the spatial differences in resistivity and polarization, it becomes feasible to easily and accurately identify oil, gas, and water. Furthermore, numerous petrophysical experiments have demonstrated that shale gas reservoirs, particularly in southern China, typically exhibit low density, low seismic velocity, high electrical resistivity, and low magnetization properties [16].

Conducting airborne geophysical surveys is essential for the exploration of vast areas to identify potential shale gas reserves. These surveys are particularly useful because shale gases have a higher electrical resistivity compared to the surrounding sedimentary layers, making airborne electromagnetic surveys a key focus in this type of exploration. An emerging technique involves utilizing electromagnetic surveys with a natural source, which shows promise in enhancing the accuracy and efficiency of identifying shale gas deposits. Labson et al. (1985) developed a method to measure the horizontal magnetic field using MT processing techniques, known as the Z-axis tipper EM (ZTEM) technique [17,18]. This technique involves connecting vertical magnetic field data H_zmeasured by a horizontal coil towed behind a helicopter or aircraft to horizontal magnetic field data (i.e. two vertical coils measuring H_x and H_y) from a ground-based reference station (Fig. 1). The ZTEM technique allows for the rapid collection of vertical magnetic field data over a large area with a mobile horizontal coil, and then tipper data are obtained through MT data processing techniques based on two fixed vertical coils measuring horizontal magnetic fields. The frequency range typically used in ZTEM surveys is 30-720 Hz, determined by flight speed and sampling rate limitations. Since its introduction, the ZTEM technique has been widely utilized in environmental engineering, mineral exploration, and hydrocarbon exploration due to its effectiveness and versatility [19-21].

The current research aims to examine the potential for exploring shale gas targets through the utilization of the ZTEM survey. This study will involve conducting simulations based on three distinct geological scenarios across 2D shallow shale models to assess the effectiveness of the electrical model in accurately predicting the recovery capacity of this unconventional reservoir. By employing numerical techniques, the geophysical model will be able to gather valuable data that can provide insights into the feasibility and viability of extracting shale gas resources. The inversion of the collected data will allow for a comprehensive evaluation of the electrical properties of the shale formations, shedding light on the potential challenges and opportunities associated with this reservoir.

2. Methodology

In the conventional 2D ZTEM problem, the earth is treated as a half-space conductor ($z \geq 0$) with an insulated air layer on top, while the electromagnetic field source is located above the surface. The electromagnetic fields are considered to be plane waves because of the considerable distances between the survey area and the transmitted fields in the ZTEM method. The Maxwell equation in its differential form assuming a quasi-static approximation is used to express this scenario as,

$$\nabla \times \mathrm{E} = -\mathrm{i}\omega\mu_0\mathrm{H} \quad (1)$$

$$\nabla \times \mathrm{H} = \sigma\mathrm{E} \quad (2)$$

The resistivity distributions remain constant along the strike direction for the 2D structures. In Fig. 2, the y-axis represents the geo-electrical strike direction, while the z direction is positive downwards. This results in two distinct polarizations, transverse electric (TE) and transverse magnetic (TM), during MT survey. The 2D Helmholtz equations are defined separately for TE and TM polarizations as,

$$\frac{\partial^2 \mathrm{E_y}}{\partial \mathrm{x}^2} + \frac{\partial^2 \mathrm{E_y}}{\partial \mathrm{z}^2} = -\mathrm{i}\omega\sigma\mu_0\mathrm{E_y} \quad \text{TE mode} \quad (3)$$

$$\frac{\partial \mathrm{E_y}}{\partial \mathrm{z}} = \mathrm{i}\omega\mu_0\mathrm{H_x} \quad (4)$$

$$\frac{\partial \mathrm{E_y}}{\partial \mathrm{x}} = \mathrm{i}\omega\mu_0\mathrm{H_z} \quad (5)$$

$$\rho\left(\frac{\partial^2 \mathrm{H_y}}{\partial \mathrm{x}^2} + \frac{\partial^2 \mathrm{H_y}}{\partial \mathrm{z}^2}\right) + \frac{\partial \rho}{\partial \mathrm{x}}\frac{\partial \mathrm{H_y}}{\partial \mathrm{x}} + \frac{\partial \rho}{\partial \mathrm{z}}\frac{\partial \mathrm{H_y}}{\partial \mathrm{z}} = -\mathrm{i}\omega\mu_0\mathrm{H_y} \quad \text{TM mode} \quad (6)$$

Here, the angular frequency is denoted by ω, while $\mathrm{E_x}$ and $\mathrm{E_y}$ represent the electrical fields (V/m) in the x- and y- directions. On the other hand, $\mathrm{H_x}$, $\mathrm{H_y}$ $\mathrm{H_z}$ stand for the magnetic fields (A/m) in the Cartesian directions. The uniform magnetic permeability of free space is $\mu_0 =$

$4\pi \times 10^{-7}$ H/m, σ is the conductivity (Siemens/m), and ρ is the resistivity (Ωm) of the medium.

In the coordinate system, let h denote the height of the helicopter, where the positive z-axis points downwards towards the earth. The description of the tipper T is as follows [22-25]:

$$H_z = T_{zx}H_x + T_{zy}H_y \quad (7)$$

Because the H_z is only in the TE mode in 2D geo-electrical structures, Eq. (7) is simplified as [26, 27]:

$$H_z = T_{zx}H_x \quad (8)$$

The 2D ZTEM forward model problem is commonly solved using the finite element, finite differential, and Green's function integral equation (GIE) method. The primary task in the forward problem is to solve the partial differential equation. To achieve this, the global matrix equation needs to be calculated for TE polarization across all frequencies as,

$$Kv = s \quad (9)$$

K is the coefficient matrix. v is composed of the unknown E_y field and s is the right vector of the equation as boundary values. After solving the equation and obtaining the auxiliary fields H_x , H_z from E_y (Eqs. 4 and 5), finally, the tipper can be obtained [22-27].

The inverse modeling of geophysical data involves the optimization of a well-posed function, as outlined by Abedi et al., 2014 [28],

$$\varphi(\mathbf{m}) = \varphi_d + \lambda\varphi_m \quad (10)$$

The misfit norm φ_d is characterized by the following form:

$$\varphi_d = \left\|\mathbf{W}_d\left(\mathbf{d}^{obs} - \mathbf{Fm}\right)\right\|_2^2 \quad (11)$$

The parameter λ represents Tikhonov regularization for balancing the model (φ_m) and misfit norms. A linear operator or a Jacobian matrix (**F**) can forward the physical property (**m**) to the tipper data. The observed data ($\mathbf{d}^{obs}$) are scaled by a diagonal matrix of $\mathbf{W}_d$ in the form of $\mathbf{W}_d = \mathrm{diag}\left(1/\sigma_1, \ldots, 1/\sigma_i \ldots, 1/\sigma_N\right)$, where σ_i denoting the level of noise affecting the ith observation [29].

In the field of inverse problem, various stabilizer functions are commonly employed (e.g., [30, 31]). One of these is the minimum support (MS) stabilizer [32], which effectively preserves the boundaries of the source by mitigating the fuzzy impact of the physical property distribution [33]. In this study, we utilize this model norm stabilizer to produce an electrical resistivity solution [34],

$$\varphi_m = \|\mathbf{W}_{Foc}(\mathbf{m} - \mathbf{m}_0)\|_2^2 \quad (12)$$

Where the prior electrical resistivity solution of the model is denoted as $\mathbf{m}_0$, and the focusing matrix $\mathbf{W}_{Foc}$ contains diagonal weights [35],

$$\mathbf{W}_{Foc} = ((\mathbf{m} - \mathbf{m}_0)^{\tau} + \alpha\mathbf{I})^{-1/2} \quad (13)$$

The focusing parameter α is typically set to a small value through trial-and-error to sharpen the physical property being constructed, while τ represents an exponent parameter. The matrix **L** acts as a simple second-difference operator, **Lm** approximating the Laplacian of $\log\rho$ when the model block grid is uniform. By combining the focusing and smoothing matrices, $\mathbf{W}_m = \mathbf{W}_{Foc}\mathbf{L}$, the L2-norm objective function is introduced as stated in references [36, 37].

$$\varphi(\mathbf{m}) = \left\|\mathbf{W}_d\left(\mathbf{d}^{obs} - \mathbf{Fm}\right)\right\|_2^2 + \lambda\|\mathbf{W}_m(\mathbf{m} - \mathbf{m}_0)\|_2^2 \quad (14)$$

Setting $\delta\varphi(\mathbf{m})/\delta\mathbf{m} = 0$, the Equations 15 and 16 are inferred at an iteration number *l* as,

$$[\boldsymbol{F}^T\boldsymbol{W}_d^2\boldsymbol{F} + \lambda^l(\boldsymbol{W}_m^l)^T\boldsymbol{W}_m^l]\delta\boldsymbol{m} = \boldsymbol{F}^T\boldsymbol{W}_d^2(\boldsymbol{d}^{obs} - \boldsymbol{F}\boldsymbol{m}^{l-1}) - \lambda^l(\boldsymbol{W}_m^l)^T\boldsymbol{W}_m^l(\boldsymbol{m}^{l-1} - \boldsymbol{m}_0) \quad (15)$$

$$\boldsymbol{m}^l = \boldsymbol{m}^{l-1} + \delta\boldsymbol{m} \quad (16)$$

The nonlinear conjugate gradient algorithm (NLCG) was used to solve Eq. 15 iteratively for updating $\mathbf{m}^l$ [24].

3. Shale Gas Reservoir Simulation

The utilization of airborne ZTEM data has been proposed as a valuable tool in the identification of various potential reservoir areas. This method involves the measurement of airborne electromagnetic data, which offers insights into the conductivity structure of the shallow subsurface. By capturing tipper data derived from the vertical component of the magnetic field, the ZTEM approach proves to be a cost-effective means of data collection, covering a wide area with a dense sampling distribution. However, it is important to note that this method is not sensitive

to 1D layers, as highlighted by Holtham and Oldenburg (2010) [38]. Furthermore, there are limitations associated with the frequencies measured, which can lead to reduced resolution in the models generated and shallow penetration depths, as discussed by Spratt et al. (2012) [39]. Despite these limitations, the acquisition of ZTEM data remains a promising technique for identifying areas with various reservoir potential. The ZTEM method allows for the measurement of data ranging from 30 Hz to 720 Hz, enabling the detection of subsurface features up to depths of 1 km or more, depending on the conductivity of the terrain. Compared to ground surveys, ZTEM surveys can cover large areas at a lower cost, making it a practical and cost-effective technique for mapping extensive geological structures. The ZTEM instrumentation involves a helicopter towing a coil, which measures the vertical component of the magnetic field at an altitude of approximately 80 m. Additionally, two vertical coils located in the reference station measure the horizontal components of the magnetic field [40, 41]. A visual representation of the system's essential components can be found in Figure 1.

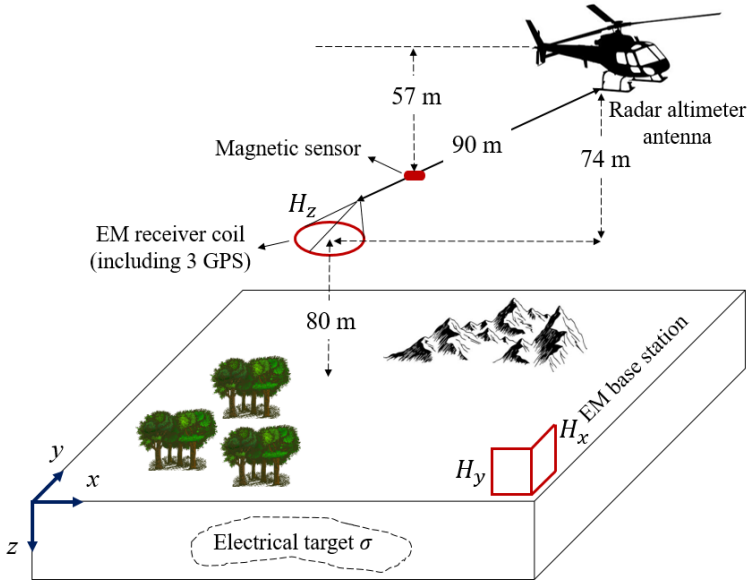

Fig. 1. Geophysical configuration of ZTEM survey with a ground-based reference station to measure horizontal magnetic fields with two vertical coils and a helicopter-borne flying horizontal coil to measure the vertical magnetic field (reproduced from Geotech Ltd.).

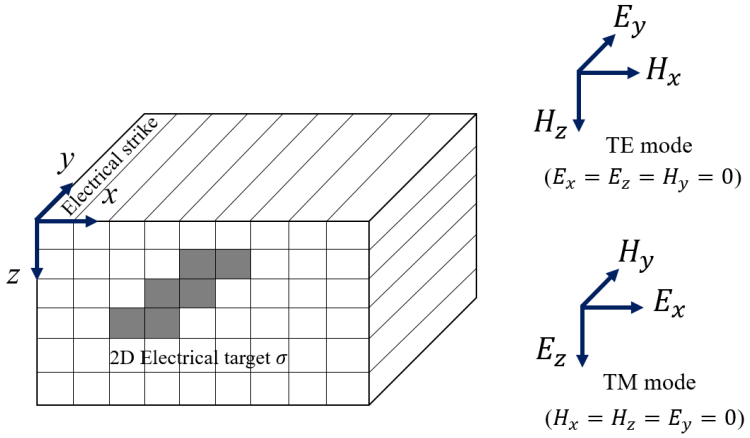

Fig. 2. A schematic representation of 2D resistivity structure with two electrical and magnetic modes.

The study involved the simulation of three distinct scenarios to assess the effectiveness of the airborne electromagnetic method in shallow shale gas exploration. The geological formations were considered to be electrically two-dimensional for the simulations. Schlumberger WingLink software was utilized to simulate the necessary data for the study. The first scenario created a synthetic model where a gas-saturated shale layer, characterized by an electrical resistivity of 100 Ωm, was embedded within a limestone sedimentary sequence with a resistivity of 50 Ωm, as illustrated in Fig. 3a. This model aimed to test the capability of the method in detecting shale gases under specific geological conditions. To streamline the modeling process and focus solely on the electromagnetic response of the formations, certain complexities were intentionally excluded from the simulations. Factors such as the composition of shale, porosity percentage, saturation degrees, clay content, and petrophysical relationships governing these properties were deliberately left out to maintain the simplicity of the study and isolate the impact of the shale gas presence on the electrical resistivity measurements. The desired layer's length is set at 1000 meters, with an assumed thickness of 200 meters. This shale block is positioned at a depth of 200 meters beneath the earth's surface. For the modeling process, it was assumed that the topography was smooth, and data collection was conducted at a height of 80 meters above the ground surface. The tipper data values were calculated within a frequency range spanning from 1 to 1000 Hz, with measurements taken at 9 different frequencies. To ensure a comprehensive analysis, three frequencies were selected at each decade in the logarithmic scale, ranging from 100 to 103. Along the 3-km profile, stations were placed at a distance of 50 meters from each other. To account for environmental and ambient noise effects, 3% random Gaussian noise was added to each set of data, ensuring a more accurate and reliable analysis. Figure 4 displays the real and imaginary tipper vector values that have been observed. These values have a range of less than 3% along the assumed profile. To analyze the ZTEM data, the aforementioned inversion algorithm was utilized through the WinGLink software. After approximately 30 iterations, the results achieved the desired level of misfit. The inversion model, as depicted in Fig. 3b, successfully recovered the assumed shale gas trap model. Furthermore, the predicted data closely aligns with the observed data values shown in Fig. 4. To obtain these results, the Lagrange coefficient (Tikhonov regularization parameter) was assumed to be one after conducting several trial and error tests. Additionally, the focusing parameter and exponent parameter values were set to 0.1 and 0.5 respectively, throughout this study.

In the second geological scenario, two distinct gas-bearing shale structures were modeled, as shown in Fig. 5a. The electrical resistivity of the shale structures was consistent with the first scenario at 100 Ωm, while the background limestone sediments were maintained at 50 ohm meters. The target on the right side was positioned at a depth of 100 meters, with dimensions of 500 meters in length and 100 meters in thickness. On the left side, the target was located at a depth of 200 meters, with dimensions of 600 meters in length and 200 meters in thickness. The necessary parameters for inverse modeling were similar to previous scenario, just the regularization parameter was set at 0.1. Real and imaginary data of the tipper vector were computed along the profile for 9 frequencies, assuming a 3% random Gaussian noise. Notably, the amplitude of the real and imaginary components remained below 3% across all frequencies (Fig. 6). The result of the inverse modeling was highly successful in accurately representing the locations of the two-shale gas-bearing structures, as depicted in Fig. 5b. Furthermore, the predicted data closely aligned with the actual data observed in Fig. 6, underscoring the reliability and precision of the modeling approach employed in this geological scenario.

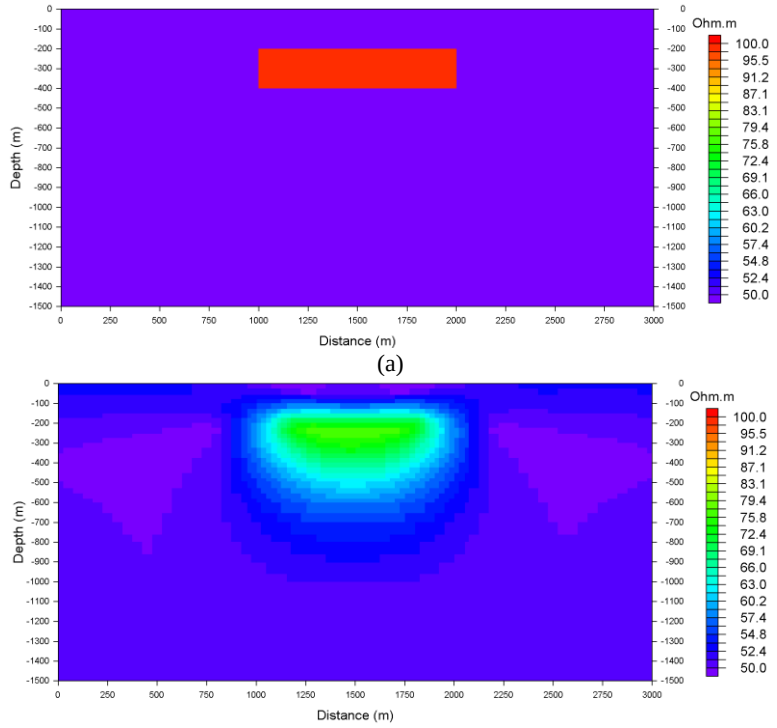

Fig. 3. First synthetic electrical resistivity scenario, (a) a thick shale gas layer, and (b) imaged resistivity model.

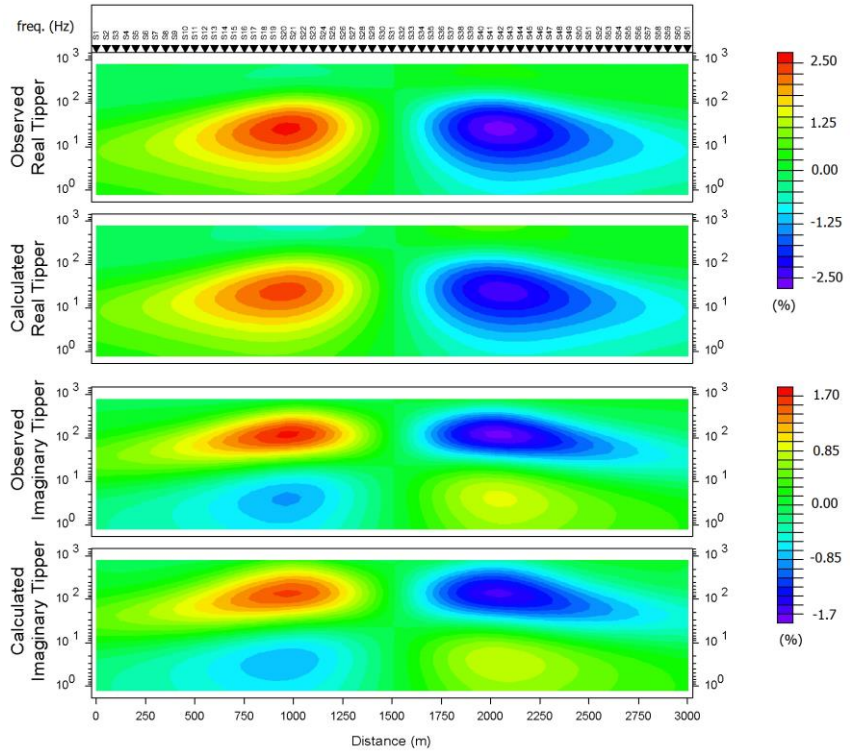

Fig. 4. Observed and predicted real and imaginary components of Tipper data at the frequency interval 1 to 1000 Hz for the first synthetic scenario.

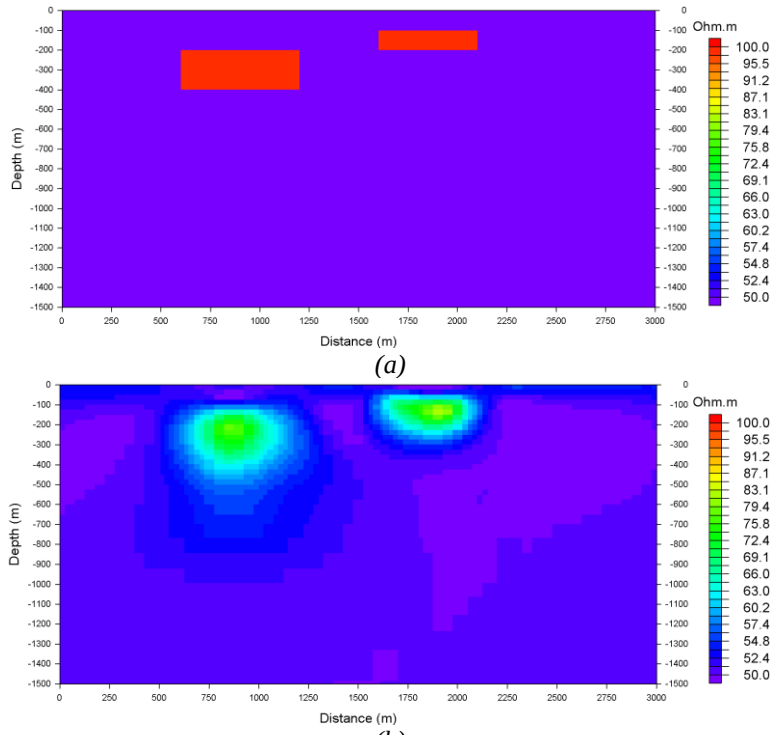

Fig. 5. Second synthetic electrical resistivity scenario, (a) two shale gas layers, and (b) imaged resistivity model.

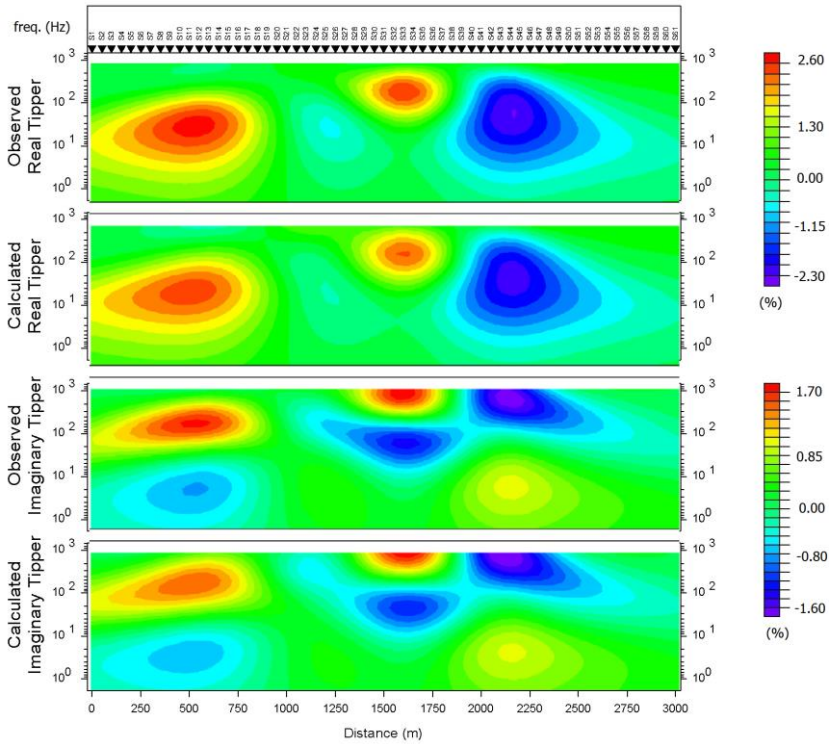

Fig. 6. Observed and predicted real and imaginary components of Tipper data at the frequency interval 1 to 1000 Hz for the second synthetic scenario**.**

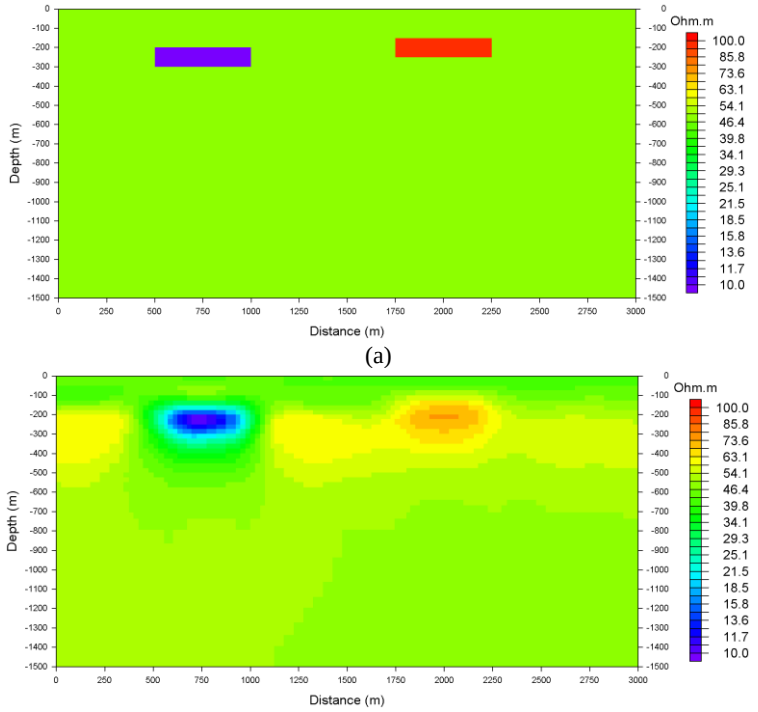

Fig. 7. Third synthetic electrical resistivity scenario, (a) two gas-free and gas-saturated shale layers, and (b) imaged resistivity model**.**

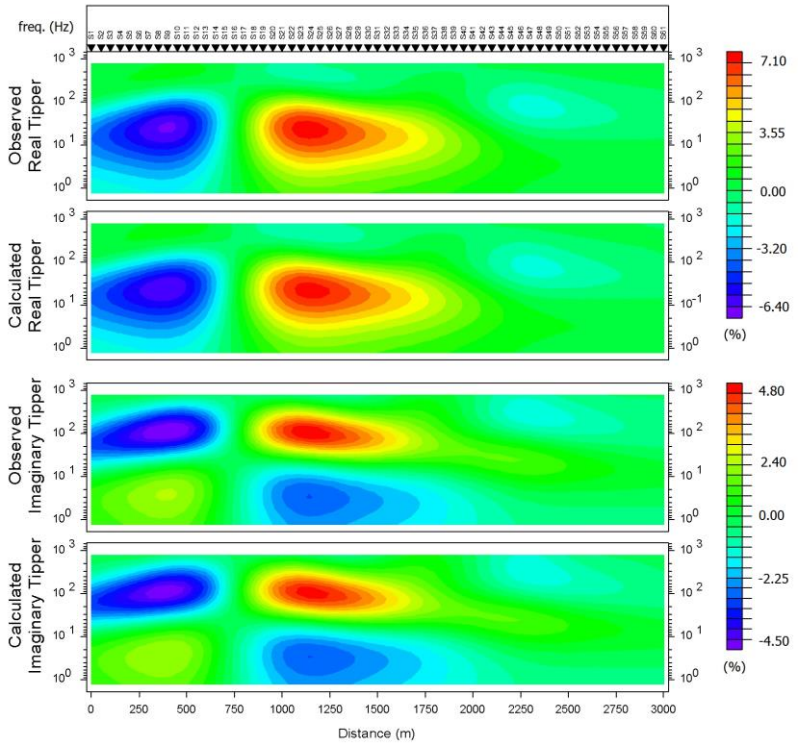

Fig. 8. Observed and predicted real and imaginary components of Tipper data at the frequency interval 1 to 1000 Hz for the third synthetic scenario.

In the third simulated case, two distinct geological structures for analysis were assumed. The structure on the right side is a gas-saturated shale formation with an electrical resistivity of 100 Ωm, situated at a depth of 150 meters. It has a length of 500 meters and a thickness of 100 meters. In addition, the structure on the left side is a gas-free shale formation with an electrical resistivity of 10 Ωm. This shale structure is located at a depth of 200 meters, with a length of 500 meters and a thickness of 100 meters, as illustrated in Fig. 7a. The data collected for these structures includes 3% random Gaussian noise, as depicted in Fig. 8. It is important to note that the range of real and imaginary components across all frequencies is less than 7%. Following the same approach as in the previous scenarios, inverse modeling was conducted, resulting in the outcome shown in Fig. 7b. Notably, the two structures are distinctly separated from each other, approving the accuracy of the analysis. The regularization parameter utilized in this case is set at 0.1, while the other parameters remain consistent with those of the initial scenario. The predictive data displayed in Fig. 8 demonstrates a close estimation of the observed data, indicating the effectiveness of the modeling approach employed. This detailed analysis provides valuable insights into the characteristics and behavior of the gas-saturated and gas-free shale structures, contributing to a deeper understanding of their electrical properties and distribution at varying depths.

Three shale gas scenarios discussed above, all make the assumption of a straightforward geological environment, overlooking the petrophysical connections within the unconventional shale gas trap. As assumed, the models generated have shown significant variations from the typical sedimentary background, ultimately enhancing the likelihood of identifying these structures. To pinpoint the location of such targets accurately within intricate geological settings, it is imperative for the inverse modeling process to establish geological constraints and other mathematical parameters [42-50]. This will enable a more precise identification of potential shale structures, paving the way for more effective exploration strategies in the future. Moving forward, it is crucial for upcoming studies to focus on simulating shale structures with a 3D geometry and within more complex geological environments. By incorporating three-dimensional inversion algorithms that enforce geological and mathematical constraints, the potential of the airborne electromagnetic tool can be maximized, offering a more comprehensive understanding of the subsurface landscape.

4. Conclusion

The research presented in this study focused on simulating unconventional shale gas reservoirs by analyzing the electrical resistivity of the underlying geological formations. Three different scenarios were considered, and the electromagnetic responses of each scenario were generated. To investigate these structures, a ZTEM survey was utilized. The responses obtained within the assumed frequency range exhibited noticeable changes in the tipper vector when compared to the background sedimentary sequence. Then, an inversion algorithm was employed to model the airborne data and accurately determine the location of the gas traps. The restored models successfully depicted the positions of these traps. However, to enhance the simulation results, it is crucial to utilize more advanced inversion tools that can provide a sharper reconstruction of the electrical models. Furthermore, to evaluate the effectiveness of natural source airborne electromagnetics survey in modeling unconventional and shallow traps, it is necessary to develop numerical simulations that consider more complex geological environments closer to reality. This will enable a comprehensive assessment of the applicability of this survey method in both two- and three-dimensional modeling of such traps.

5. Acknowledgment

I am deeply grateful to the School of Mining Engineering at the University of Tehran for their unwavering support and assistance.

6. References

[1] Caineng, Z., Zhi, Y., Zhang, G., Lianhua, H., Rukai, Z., Shizhen, T., Xuanjun, Y., Wang, Y., Guo, Q., WANG, L., & Haibin, B.I., (2014) Conventional and unconventional petroleum “orderly accumulation”: concept and practical significance. Pet Explor Dev., 41(1):14-30.

[2] Muther, T., Qureshi, H.A., Syed, F.I., Aziz, H., Siyal, A., Dahaghi, K., & Negahban, S., (2022). Unconventional hydrocarbon resources: geological

statistics, petrophysical characterization, and field development strategies. J Petrol Explor Prod Technol., 12, 1463-1488.

[3] Song, Y., Li, Z., Jiang, L., & Hong, F., (2015). The concept and the accumulation characteristics of unconventional hydrocarbon resources. Pet Sci., 12(4), 563-572.

[4] Hamada, G.M., (2016). Comprehensive Evaluation and Development of Unconventional Hydrocarbon Reserves as Energy Resource. Petro and Envi Biotech., APEB-102.

[5] Heikal, S., (2008). Scope of Tight Gas Reservoir in Pakistan. Pakistan Petroleum Exploration & Production Companies Association (PPEPCA), Islamabad, Pakistan.

[6] Sondergeld, C. H., & Rai, C.S., (2011), Elastic anisotropy of shales: The Leading Edge, 30, 324-331.

[7] Roth, M., 2010, Shale gas reservoirs - similar, yet so different: 3D seismic symposium.

[8] Huang, T., Xie, B., Ran, Q., Zou, D., & Zhong, G., (2015). Geophysical evaluation technology for shale gas reservoir: A case study in Silurian of Changning Area in Sichuan Basin. ENERGY EXPLORATION & EXPLOITATION, 33 (3), 419-438.

[9] Kumar, D., & Hoversten, M., (2012). Geophysical model response in a shale gas. 9th Biennial International Conference & Exposition on Petroleum Geophysics. Hyderabad, 1-7.

[10] Nazarenko, M.Y., Kondrasheva, N., & Saltykova, S.N., (2018). Electrical Resistivity of Coal and Oil Shales. Coke and Chemistry, 61(5), 184-187.

[11] Senger, K., Birchall, T., Betlem, P., Ogata, K., Ohm, S., Olaussen, S., & Paulsen, R.S., (2021). Resistivity of reservoir sandstones and organic rich shales on the Barents Shelf: Implications for interpreting CSEM data, Geoscience Frontiers, 12 (6), 101063.

[12] Spichak, V., (2018). Advances in electromagnetic techniques for exploration, prospecting, and monitoring of hydrocarbon deposits. First Break, 36(10), 75-81.

[13] Constable, S., Srnka, L.J., (2007). An introduction to marine controlled-source electromagnetic methods for hydrocarbon exploration. Geophysics, 72, WA3-WA12.

[14] Strack, K.M., (2012). Future Directions of Electromagnetic Methods for Hydrocarbon Applications. Surv Geophys, 35, 157–177.

[15] He, Z., & Wang, X., (2007). Geo-electrical anomalous pattern of reservoir and oil/gas detection by electromagnetic survey. Oil Geophysical Prospecting, 42(1), 102-106.

[16] Mingfei, W., Chao, C., Dapeng, Q., et al., (2015). The geophysical characteristics of shale gas reservoir from Wufeng member to Longmaxi member in Jiaoshiba block of Fulin shale gasfield. Geophysical Prospecting for Petroleum, 54(5), 613-620.

[17] Labson, V.F., Becker, A., Morrison, H.F., & Conti, U., (1985). Geophysical exploration with audiofrequency natural magnetic fields. Geophysics, 50 (4), 656-664.

[18] Legault, J., Wilson, G.A., Gribenko, A.V., Zhdanov, M.S., Zhao, S., & Fisk, K., (2012). An overview of the ZTEM and AirMt airborne electromagnetic systems: A case study from the Nebo-Babel Ni-Cu-PGE deposit, West Musgrave, Western Australia. Preview, 158, 26-32.

[19] Pellerin, L., (2002). Applications of electrical and electromagnetic methods for environmental and geotechnical investigations. Surv. Geophys., 23 (2-3), 101-132.

[20] Jefferson, C.W., Thomas, D.J., Gandhi, S.S., Ramaekers, P., & Olson, R.A., (2007). Unconformity-associated uranium deposits of the Athabasca Basin, Saskatchewan and Alberta. Geological Assoc. Canada, Mineral Deposits Division, Special Publication, St. John's, NF, Canada, Tech. Rep. 273305.

[21] Witherly, K., & Sattel, D., (2012). The application of ZTEM to porphyry copper-gold exploration. ASEG Extended Abstr., vol. 2012, no. 1, pp. 1-4.

[22] Nabighian, M.N. (Ed.)., (1988). Electromagnetic methods in applied geophysics: Volume 1, theory. Society of Exploration Geophysicists.

[23] Nabighian, M.N., (1991). Electromagnetic methods in applied geophysics: Volume 2, application parts A and B. Society of Exploration Geophysicists.

[24] Rodi, W., & Mackie, R.L., (2001). Nonlinear conjugate gradients algorithm for 2-D magnetotelluric inversion. Geophysics, 66, 174-187.

[25] Zhdanov, M.S., (2017). Foundations of geophysical electromagnetic theory and methods (Vol. 43). Elsevier.

[26] Özyıldırım, Ö., Candansayar, M.E., Demirci, İ., & Tezkan, B., (2017). Two-dimensional inversion of magnetotelluric/radiomagnetotelluric data by using unstructured mesh. Geophysics, 82(4), E197-E210.

[27] Wang, M., Tan, H., Wang, Y., Lin, C., & Peng, M., (2022). Parallel Computation for Inversion Algorithm of 2D ZTEM. on Algorithm of 2D ZTEM. Appl. Sci., 12, 12664.

[28] Abedi, M., Gholami, A., & Norouzi, G.H., (2014). 3D inversion of magnetic data seeking sharp boundaries: a case study for a porphyry copper deposit from Now Chun in central Iran. Near Surface Geophysics, 12 (5), 657-666.

[29] Oldenburg, D.W., & Li, Y., (2005). Inversion for applied geophysics: a tutorial. In: Butler, D.K. (Ed.), Near-surface Geophysics: pp. 89-150 (SEG.)

[30] Gundogdu, N.Y., & Candansayar, E., (2018). Three-dimensional regularized inversion of DC resistivity data with different stabilizing functionals. Geophysics, 83 (6), E399-E407.

[31] Xiang, Y., Yu, P., Zhang, L., Feng, S., & Utada, H., (2017). Regularized magnetotelluric inversion based on a minimum support gradient stabilizing functional. Earth, Planets and Space, 69,158.

[32] Last, B.J., & Kubik, K., (1983). Compact gravity

inversion. Geophysics, 48, 713-21.
[33] Farquharson, C.G., (2008). Constructing piecewise-constant models in multidimensional minimum-structure inversions. Geophysics, 73, K1-K9.
[34] Huang, X.Y., Deng, J.Z., & Chen, X., (2019). Magnetotelluric extremum boundary inversion based on different stabilizers and its application in a high radioactive waste repository site selection. Appl Geophys., 16, 367-377.
[35] Zhdanov, M.S., (2002). Geophysical Inverse Theory and Regularization Problems (Amsterdam: Elsevier).
[36] Abedi, M., (2020). A focused and constrained 2D inversion of potential field geophysical data through Delaunay triangulation, a case study for iron-bearing targeting at the Shavaz deposit in Iran. Physics of the Earth and Planetary Interiors, 309, 106604.
[37] Abedi, M., (2022). Cooperative fuzzy-guided focused inversion for unstructured meshmodeling of potential field geophysics, a case study for imagingan oil-trapping structure. Acta Geophysica, 70, 2077-2098.
[38] Holtham, E., & Oldenburg, W., (2010). Three-dimensional inversion of ZTEM data; Geophysical Journal International, 182, 168-192.
[39] Spratt, J.E., Farquharson, C.G., & Craven, J.A., (2012). Analysis of Magnetotelluric Transfer Functions to Determine the Usefulness ofZTEM Data in the Nechako Basin, South-Central British Columbia (Parts of NTS092O, N, 093B, C, F, G). Geoscience BC Report 2012-1.
[40] Cao, X., Huang, X., Yin, C., Yan, L., & Han, Y., (2022). 3-D Inversion of Z-Axis Tipper Electromagnetic Data Using Finite-Element Method with Unstructured Tetrahedral Grids. IEEE TRANSACTIONS ON GEOSCIENCE AND REMOTE SENSING, 60, 5904811.
[41] Han, M., (2017). THREE-DIMENSIONAL INVERSION OFAIRBORNE ZTEM AND AIRMT DATA. MSc Thesis, The University of Utah, 82 p.
[42] Fayemi, O., & Di, Q., (2016). 2D Multitransient Electromagnetic Response Modeling of South China Shale Gas Earth Model Using an Approximation of Finite Difference Time Domain with Uniaxial Perfectly Matched Layer. Hindawi Publishing Corporation, Discrete Dynamics in Nature and Society, 6863810, 20 p.
[43] Holditch, S.A., (2013). Unconventional oil and gas resource development - let's do it right. J. Unconv. Oil Gas Resour., 1-2, 2-8.
[44] MacGregor, L., & Tomlinson, J., (2014). Marine controlled-source electromagnetic methods in the hydrocarbon industry: a tutorial on method and practice. Interpretation, 2 (3), SH13-SH32.
[45] Strack, K.M., (1999). Exploration with Deep Transient Electromagnetics, Elsevier Scientific, Amsterdam, The Netherlands.
[46] Vedachalam, N., Srinivasalu, S., Rajendran, G., Ramadass, G.A., & Atmanand, M.A., (2015). Review of unconventional hydrocarbon resources in major energy consuming countries and efforts in realizing natural gas hydrates as a future source of energy. Journal of Natural Gas Science and Engineering, 26, 163-175.
[47] Xue-Li, Y., Bo, L., Chuan-Sheng, P., & Yang, Y., (2017). Application of a wide-fi eld electromagnetic method to shale gas exploration in South China. Applied Geophysics, 14 (3), 441-448.
[48] Yan, L., (2022). Electromagnetic technology for prospecting unconventional hydrocarbon resources. 25 th EM Induction Workshop, Çeşme, Turkey, September 11-17.
[49] Ziolkowski, A., (2007). Developments in the transient electromagnetic method. First Break, 25 (6), 99-106.
[50] Sattel, D., Witherly, K., & Kaminski, V., (2019). A brief analysis of MobileMT data. SEG International Exposition and 89th Annual Meeting, 2138-2142.